THE ASTROPHYSICAL JOURNAL, 355:427–435, 1990 June 1

FLOW PATTERNS IN RADIO HOT SPOTS: A STUDY OF 3C 33 NORTH

LAWRENCE RUDNICK AND MARTHA ANDERSON
Department of Astronomy, University of Minnesota
Received 1989 August 14; accepted 1989 December 6

ABSTRACT

High-resolution (0".36, 0.41 kpc) observations of the northern hot spot of the radio galaxy 3C 33 show a symmetric "mushroom cap" structure, with a centrally placed H-shaped feature and two opposed small bright regions. We explore two models for the flow patterns in this hot spot. First is the "splash" picture, in which the brightest compact feature is identified as the primary hot spot and the rest of the structures result from the jet's expanded, deflected flow. Although most observed features are consistent with this picture, they do not help discriminate against alternative models. The second, axisymmetric, picture compares the observations with numerical simulations of jets with helical magnetic fields. We find good agreement with the geometrical and magnetic field properties, although significant questions remain about the synchrotron emissivity characteristics. We briefly discuss the differences between the northern and southern hot spots of 3C 33, and we suggest that there are no good explanations for these differences in the context of current models.

Since the maps of 3C 33's hot spots are among the most detailed available, they demonstrate that other claims about observed flow patterns must be critically examined.

Subject headings: galaxies: individual (3C 33) — galaxies: jets — galaxies: structure — radio sources: galaxies

I. INTRODUCTION

The study of hot spots has taken on a new dimension with the current generation of radio interferometer maps. Early studies of powerful radio galaxies and quasars found bright, compact ($\lesssim 10$ kpc) regions at the extreme ends of the source (e.g., Hargrave and Ryle 1974), which came to be called hot spots. The hot spot remains a key component of today's models of luminous radio sources and is generally recognized as the place where the jet from the nucleus "dumps" its energy, perhaps converting bulk kinetic energy into synchrotron emissivity.

One of the important current observational challenges is to use these emissivity patterns to determine the underlying flow patterns and learn more about the critical interface through which the radio source is powered. However, high-resolution observations of hot spots (e.g., Dreher, Carilli, and Perley 1987) have shown them to be complex structures, making the task of establishing the flow patterns very difficult. In the southern lobe of 3C 33, we found a simple overall structure which could be modeled without resorting to collisions with ad hoc ambient clouds or beam irregularities. The 3C 33 South model was that of a bow shock, and we wished to see whether a similar model could be applied to the northern hot spot. Instead, our new VLA observations showed a dramatically different structure, but one that had its own internal order. In this paper, we present those observations and discuss two models of the flow patterns in 3C 33 North. We also comment on the limitations of our current models for synchrotron emissivity as well other factors which give such a broad range of hot spot structures.

II. OBSERVATIONS AND RESULTS

a) *Observations and Initial Analysis*

Data were taken in both the standard A- and B-configurations of the Very Large Array (VLA[1]). Approximately 4 hr and 1 half-hour integration times, on 1986 June 5 and July 13, respectively, were accumulated at a center frequency of 4835.1 MHz with a bandwidth of 50 MHz. The data were calibrated in a standard fashion, using 0106+013 as a phase and instrumental polarization calibrator and 3C 286 for amplitude (Baars *et al.* 1977 scale) and polarization position angle calibrations. The pointing center was at $01^h06^m17^s.5$, 13°06′04″, slightly south of the brighter regions of the northern hot spot. A separate set of observations pointed at the southern lobe were reported in Rudnick (1988).

Several self-calibration passes, including a final pass for both phase and amplitude corrections, were performed on each data set (A and B) separately. The brightness of the central component and southern lobe of 3C 33 required that those fields be mapped and deconvolved simultaneously, which we did using the routine MX in AIPS (the NRAO Astronomical Image Processing System), using a Sun 3/160 at the University of Minnesota. These MX maps were used as the intermediary maps for self-calibration as well as the final maps shown here. After self-calibration, the visibility data sets were concatenated to produce the final high-resolution maps, while the B-configuration data alone were used for the 1".3 maps.

b) *Results*

The parent galaxy of 3C 33 is an isolated DE4 (Mathews, Morgan, and Schmidt 1964) with a redshift of 0.059 (Simkin 1979). We use $H_0 = 75$ km s^{-1} Mpc^{-1} and $q_0 = 0.5$ throughout this paper, resulting in a scale of 1.14 kpc arcsec^{-1}. The overall radio source is a 250″ (286 kpc) triple (Hargrave and McEllin 1975), and more detailed maps of the southern lobe can be found in Rudnick (1988, hereafter R88).

Figure 1 is a gray-scale image of the northern hot spot region at a resolution of 0".36. The overall appearance of the source is that of a mushroom cap, with brighter regions at both edges of the cap (features A and B), and an unusual H-shaped structure (feature C) roughly centered within the hot spot region. This overall structure has not been seen in other hot spots, although only a few have yet been mapped with such high linear resolution. In Figure 1, we indicate the extrapolated

[1] The VLA is a facility of the National Radio Astronomy Observatory, which is operated by Associated Universities, Incorporated, with funding from the National Science Foundation.

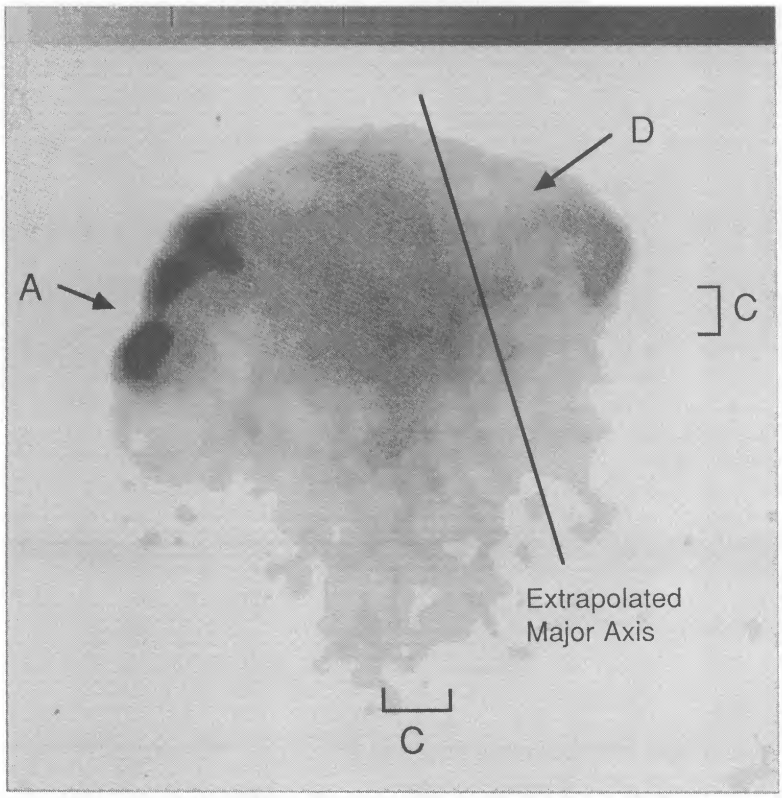

FIG. 1.—Gray-scale image of $\lambda 6$ cm total intensity of 3C 33 North. The nominal 0".36 resolution was degraded slightly in this image by a single-pass application of a median filter box with sides of length 0".3. The gray scale ranges from 45 μJy beam^{-1} (*white*) to 4.5 mJy beam^{-1} (*black*). Letters indicate features described in Table 1, and the extrapolated major source axis is explained in the text.

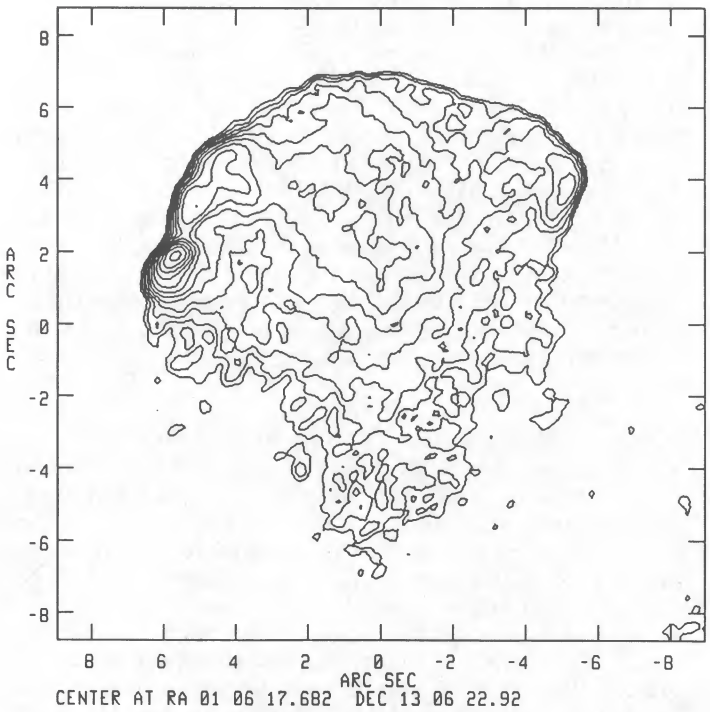

FIG. 2a

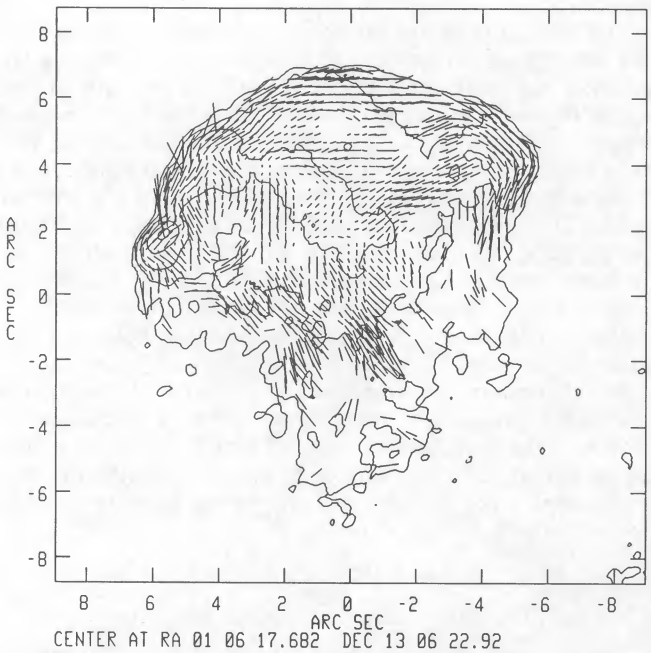

FIG. 2b

FIG. 2.—(*a*) Contours of $\lambda 6$ cm total intensity of 3C 33 North at a resolution of 0".36. The contour levels are at $0.22 \times (-1, 1, 1.5n)$ mJy beam^{-1}. (*b*) Same as (*a*) except that contour levels are at $0.22 \times (-1, 1, 3n)$ mJy beam^{-1}. Polarization vectors are overlaid, with their direction indicating the local inferred *magnetic* field and their length indicating fractional polarization with a scale of 1" = 55%.

major axis of 3C 33, determined by the line connecting the peak of the southern hot spot and the central component, and several locations in the source where physical parameters were estimated. Figure 2 shows the 0".36 resolution total intensity map, alone in (*a*), and overlaid in (*b*) with vectors whose length is proportional to the local fractional polarization and whose orientation represents that of the magnetic field. Figure 3 shows the polarization structure in more detail around the bright regions (*a*) at the eastern end and (*b*) at the western end. The rms noise on the Stokes *I*, *Q*, and *U* maps were 45, 39, and 43 μJy beam^{-1}, respectively. Within the noise, systematic structures were still visible, which might be due to incomplete cleaning of the heavily delay beam–smeared and undersampled southern lobe.

Figure 4 shows further details around the H feature (C in Fig. 1). Panel (*a*) is a gray-scale image of the total intensity, and panel (*b*) shows the total intensity and polarization structure as in Figure 3. Panel (*c*) shows an intensity cut through the center of the H feature along an axis of 12° (as discussed below). In Figure 5, the 1".3 resolution map is shown, overlaid with fractional polarization/magnetic field vectors.

c) *Estimation of Physical Parameters*

For purposes of comparison with other sources, we calculated the luminosities, emissivities, and minimum pressures of various features in 3C 33 north. These are given in Table 1. We assumed a constant spectral index of −0.74 with low- and high-frequency cutoffs of 10^7 and 10^{11} Hz, respectively. The errors introduced by uncertainties in these assumptions are small compared to those resulting from the unknown three-dimensional geometry and filling factors (assumed here = 1). In general, all these values are at the low end of the values for hot spots in Fanaroff and Riley (1979) type II sources.

III. DISCUSSION

a) *Determining Fluid Flow Patterns in Hot Spots*

The purpose of this discussion is to examine the possible flow patterns in the well-resolved hot spot region of 3C 33 North. The flow patterns must be understood before other physical questions such as the magnetic field evolution, relativistic particle acceleration, and possible other plasma effects can be addressed. To the extent possible, we will separate our discussion of the structure and dynamics of the hot spot from questions regarding its synchrotron emissivity. Unfortunately, we cannot analyze the observational data without making some assumptions and/or models of these other factors.

The following assumptions are therefore implicit in the discussion, although none of them are established observationally:

1. The relativistic particles which produce synchrotron radiation are all found within the contact discontinuity, i.e., mixed in with the outflowing material, as opposed to also illuminating the bow shock region (see R88).

2. All dynamical time scales are *short* compared to the acceleration and radiative lifetimes of the synchrotron electrons. Observed features are therefore indicative of pressure and other variations in the flow (*pressure-limited features*) as opposed to being determined by the energy gains and losses of individual particles (*radiation-limited features*). An alternative to this assumption will be discussed in § III*e*.

3. The relativistic fluid is energetically and dynamically unimportant, as are large-scale currents and/or other plasma effects.

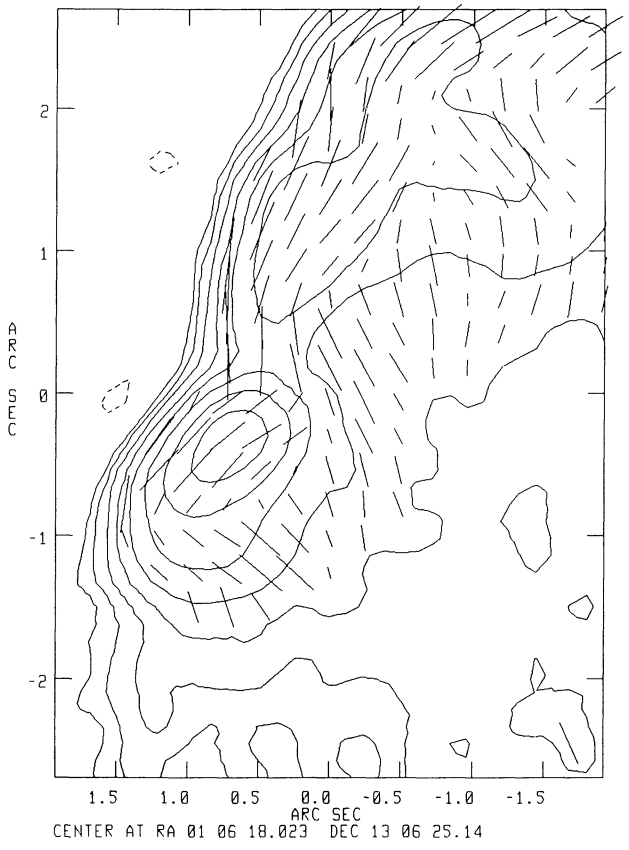

FIG. 3*a*

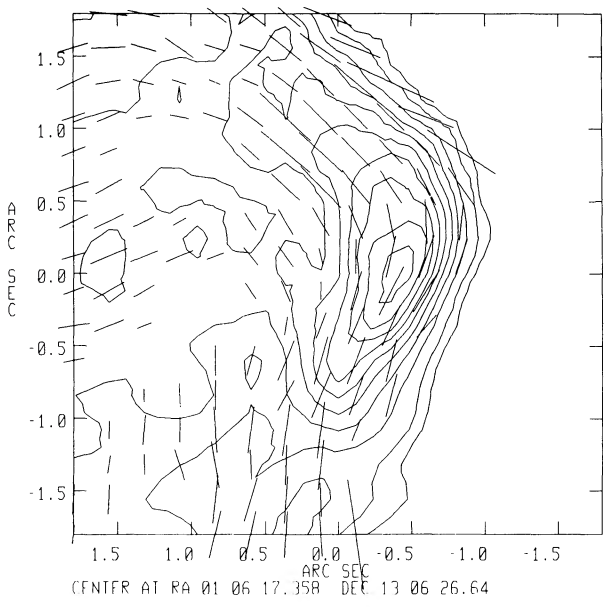

FIG. 3*b*

FIG. 3.—Closeup views of total intensity and fractional polarization, as in Fig. 2, for features A (*a*) and B (*b*). Contour levels and scales are as follows: (*a*) 0.11 × (−1, 1, 2n) mJy beam^{-1}. 1" = 83% polarization. (*b*) 0.11 × (−1, 1, 2n) mJy beam^{-1}. 1" = 111% polarization.

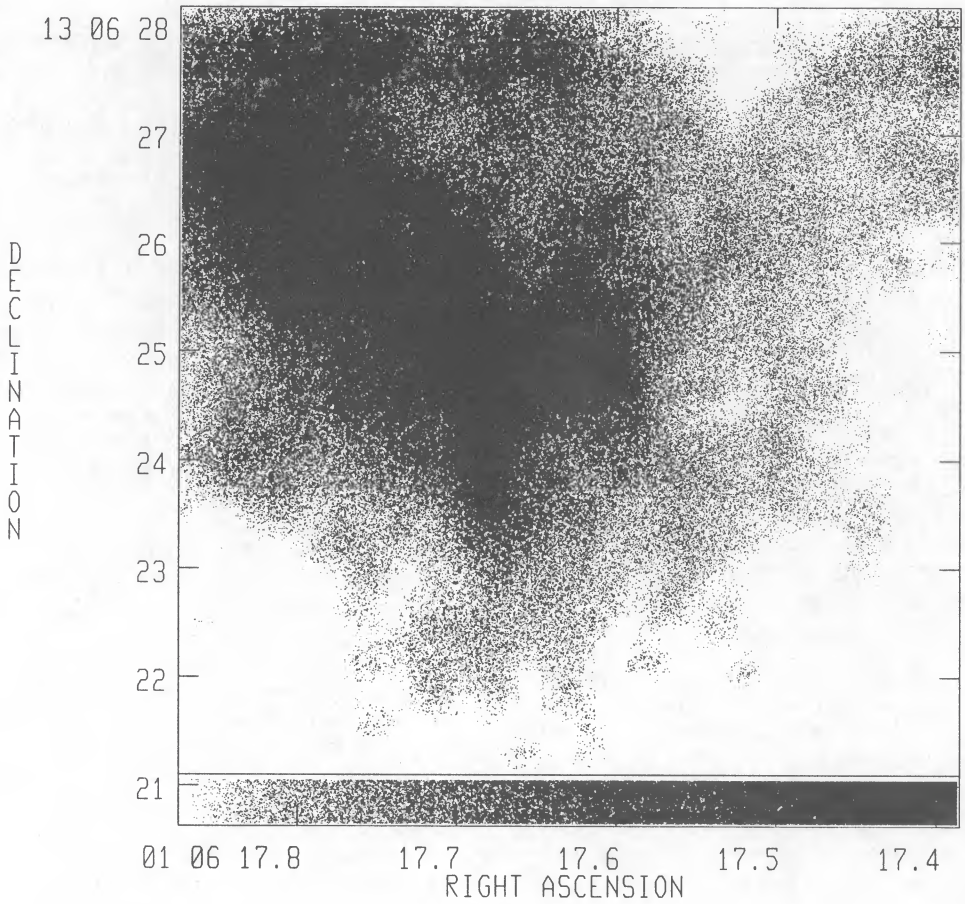

FIG. 4*a*

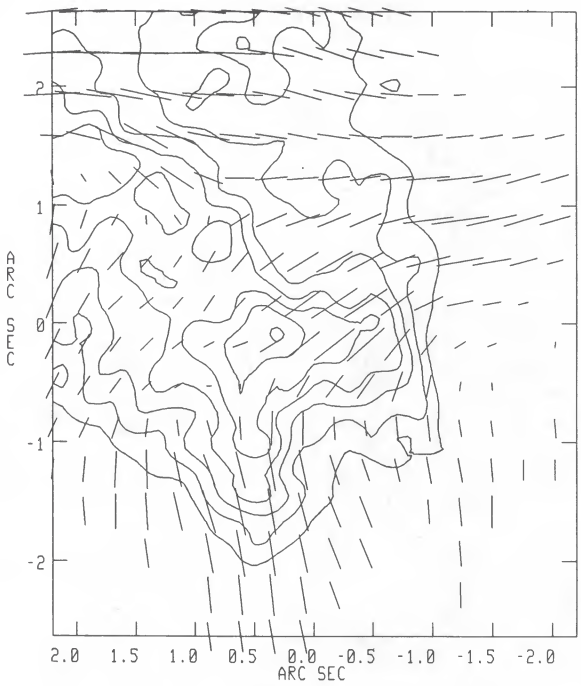

FIG. 4*b*

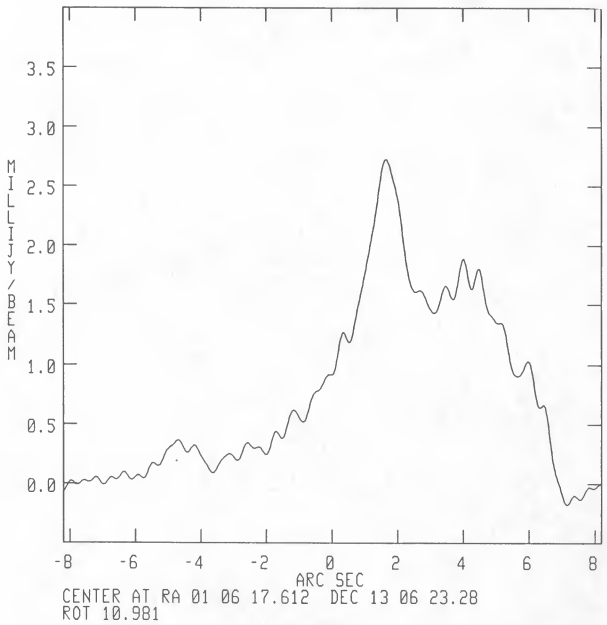

FIG. 4*c*

FIG. 4.—Details of the H region centered on feature C, λ6 cm total intensity, 0.″36 resolution. (*a*) Gray scale, with range of 0.65 mJy beam^{-1} (*white*) to 3.0 mJy beam^{-1} (*black*). (*b*) Contours at 0.25 × (5, 6, 7, 8, 9, 10, 11) mJy beam^{-1}. Polarization amplitude vectors, with *magnetic* field directions and 1″ = 2.1 mJy beam^{-1}. (*c*) Slice through the H region at a position angle of 11°. Position 0 corresponds to $01^h06^m17^s.612$, 13°06′23.″3. North is to the right, and the nucleus is to the left.

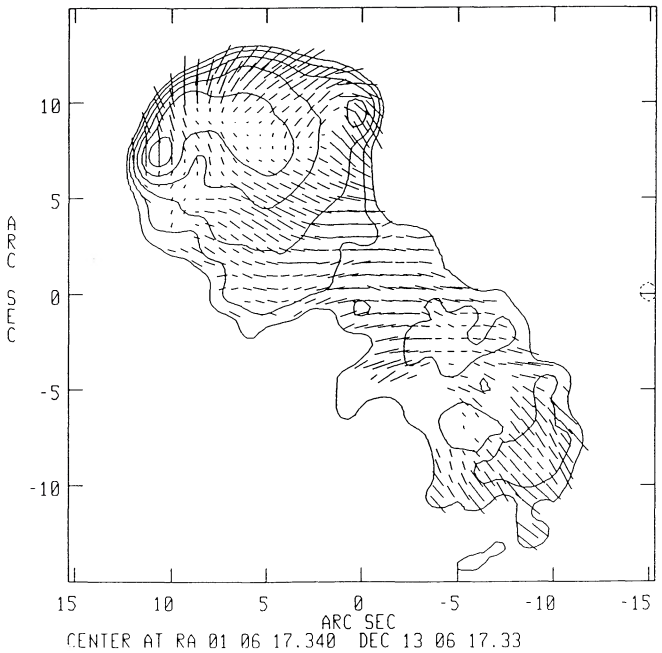

FIG. 5.—Total intensity and polarization λ6 cm map at 1″.3 resolution. Contour levels are at 1.36 × (−1, 1, 2n) mJy beam^{-1}. Polarization vectors indicate magnetic field directions and fractional polarizations, with 1″ = 30%.

Given these uncertain assumptions, it is unreasonable to expect any contemporary discussions of hot spot flow properties to reach firm conclusions. It is therefore important to develop observational tests for these assumptions. At the same time, we feel that current discussions of hot spot flows are a necessary and useful exercise.

b) *Two Pictures of Flow Patterns*

In general, the complexity of hot spot regions has not allowed identification of the streamlines, which are critical to discussions of energy transport, as well as the interaction history of the fields and relativistic particles. One clear type of hot spot has emerged—the primary plus "splash" or secondary spot (Lonsdale and Barthel 1986), for which a series of empirical rules can be listed. In these cases, a narrow jet is strongly shocked, producing the compact, primary hot spot. The jet subsequently expands and propagates through a much larger hot spot region. Below, we will examine how models of this type could be applied to 3C 33 North.

An alternative picture of flow patterns is found in the numerical simulations of axisymmetric jets. Here, by contrast, we are examining structures only a few jet diameters across. The fluid encounters a terminal shock as it enters the hot spot region and then fountains (bifurcating as seen in two dimensions) until the stagnation region, where a cocoon begins to form. Looking at the small-scale details, one finds that the observable structures are strongly dependent on the magnetic field geometry and the viewing angle (Clarke, Norman, and Burns 1989, hereafter CNB), as well as on the flow patterns.

Because the jet is not visible in 3C 33 North, it is not possible to directly determine whether we are looking at (*a*) a primary hot spot and diffuse lobe or (*b*) a wide jet of dimensions comparable to the entire observed hot spot region. We can try to use the apparent opening angle of the hot spot to decide between these two possibilities. The size of this region is $\approx$12 kpc, subtending an opening angle of approximately 4° at the nucleus. This is consistent with the spreading rate of jets for sources with total luminosities similar to that of 3C 33 (Bridle 1986). Therefore, we could argue that the jet is as broad as the entire hot spot region. In addition, numerical simulations show that the terminal jet regions are typically 3–4 jet diameters across (e.g., Smith *et al.* 1985, hereafter SNWS), so even a jet opening angle as small as 1° would be consistent with this interpretation. On the other hand, the observations of thin streams and apparent compact primary hot spots (e.g., Cygnus A: Carilli, Dreher, and Perley 1989) imply opening angles as small as 0°.2 and would support a primary plus splash picture for 3C 33 North.

Below, we discuss how each of the two models could be applied to 3C 33 North. We discuss the axisymmetric models in more detail, because so little work has been presented on them to date and because we believe that they provide a more comprehensive interpretation of the observations. We will concentrate on the geometrical, structural features and the magnetic field patterns, deferring to § III*e* a fuller discussion of the current shortcomings of arguments based on the synchrotron emissivity.

c) *The Primary plus "Splash" Picture*

A variety of models of this type exist (Scheuer 1982; Williams and Gull 1985; Lonsdale and Barthel 1986). We start by looking at the properties of the brightest, most compact part of

TABLE 1

DERIVED PHYSICAL PARAMETERS FOR 3C 33 NORTH

Label	Feature	Size[a] (kpc)	Geometry	Emissivity ($\times 10^{-26}$ ergs s^{-1} cm^{-3})	Minimum Pressure ($\times 10^{-11}$ ergs cm^{-3})
A.....	Compact peak	0.5	Ellipsoid	2300	90
		4.0	Torus[b]	300	28
B.....	Secondary peak	6.4	Torus	18	5.6
C.....	H-central bar	1.7	Oblate disk	100	15
		1.0	Prolate disk	170	20
D.....	Diffuse lobe	7.9	Solid hemisphere	3	2.5
			Hemispherical shell	11	4.1
	SW tail	7.3	Filled cylinder	1.3	1.3

NOTE.—Letters refer to labels in Fig. 1. SW tail values were taken from the map shown in Fig. 5.

[a] The actual emissivities and minimum pressures were calculated from an assumed column with the cross sectional area of the beam (FWHM = 0.42 kpc for A–D and 1.6 kpc for the tail), and a length equal to the value quoted in this column.

[b] The thickness of the torus (and the calculated path length through it) were estimated from a cross sectional profile across the peak.

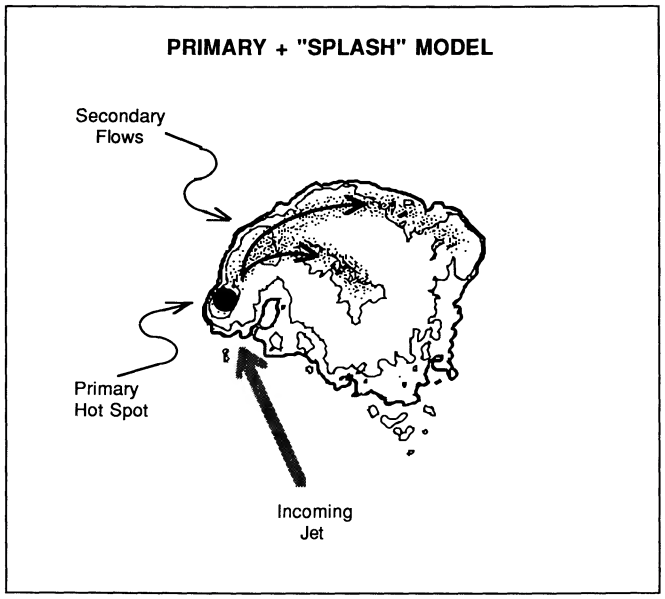

FIG. 6a

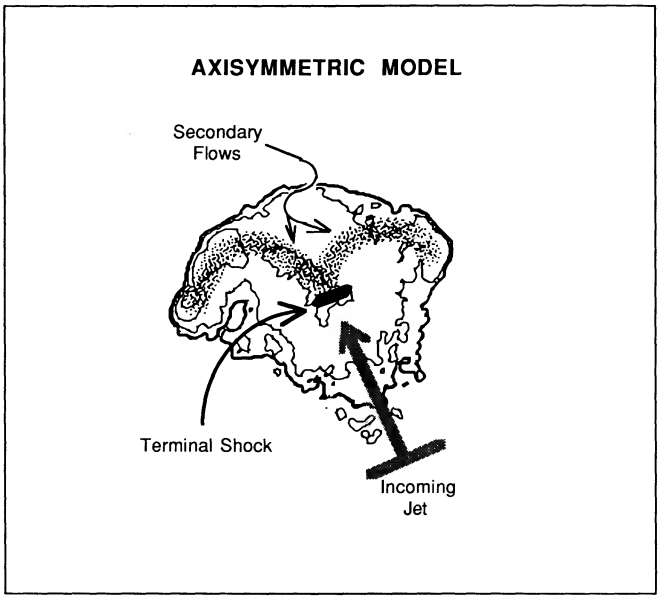

FIG. 6b

FIG. 6.—Schematics of flow models for 3C 33 North

the hot spot region and identify it (for the purposes of this discussion) as the "primary" hot spot, where the (invisible) jet ends. Figure 6*a* shows one flow pattern for 3C 33 North which fits this description.

Laing (1989) has summarized the properties of primary hot spots (from those found in a sample of 62 3C sources), which we now compare with 3C 33 North:

1. *Location.*—Primary hot spots are often found along the edge, but not at the extreme end, of the hot spot region. This is true for 3C 33 North. Primaries tend to lie on the major source axis (Lonsdale 1989). In 3C 33 North, this is not the case: the line connecting the peak of the southern lobe and the galaxy nucleus extrapolates to a position 1".5 from the center of the H feature (0°.6 projected angle at the nucleus). The primary is then 7".5 ($\approx 3°.2$) off axis.

2. *Sizes.*—They range from 0.7–2.7 kpc. 3C 33 North, at ≈ 0.5 kpc, is at the small end of this range.

3. *Other emission.*—Primary hot spots are usually significantly brighter than anything else in the region. In 3C 33 North, the primary is ≈ 5 times brighter than the next brightest feature, the region extending from the primary along the NE leading edge.

4. *Minimum pressures.*—They range from 5×10^{-8} ergs cm^{-3} to 2×10^{-6} ergs cm^{-3}. 3C 33 North's primary is two orders of magnitude lower than this lowest value and about one order of magnitude fainter than in Cygnus A (Carilli, Dreher, and Perley 1989).

5. *Extension.*—This is usually along the source axis and/or toward the brightest parts of neighboring emission. 3C 33 North fits the second of these descriptions, being extended along the edge of the source, where other bright emission is found.

6. *Flaring.*—A curved region of expanding emission from the primary. This is a good description of 3C 33 North. Other primaries are observed to be associated with a more diffuse secondary spot.

7. *Magnetic fields.*—They appear projected orthogonal to the source axis or along the line connecting the primary with other bright emission. The latter is true for 3C 33 North.

8. *Jets.*—If detected, they connect the primary to the nucleus. No jet has yet been detected for 3C 33 North.

9. *Spectral index.*—It is usually flatter than the fainter, secondary component. No detailed spectral information is yet available for 3C 33 North.

We thus find that the properties of 3C 33 North's proposed primary hot spot are generally consistent with those of primaries seen in more luminous sources, although the minimum pressures are significantly smaller. A much higher brightness peak is found in the southern lobe, although it clearly does not fit the "primary hot spot" picture.

As a further evaluation of this model, we must look at the other structures in the hot spot region. If the primary is a long-lived shock structure, then the rest of the region is filled out by the secondary flow through the primary. We must then choose whether to dismiss the H and the weaker hot spot as (*a*) accidental irregularities, turbulent regions, etc., or (*b*) natural parts of the flow structure. The second suggestion is not viable because a jet cannot be deflected by more than $\approx 130°$ before the Mach angle increases faster than the bending, and the jet is disrupted (Icke 1989). It will therefore not develop the shocks necessary to produce the H and weaker hot spot at apparent directions of 180° from the original flow. If the primary is long-lived, then these other features should thus be interpreted as accidental in this model.

If, instead, the primary is a more transient feature, as implicit in the "dentist's drill" model and its descendents, any of the features in the hot spot region can probably be explained. However, invocation of this model in this case carries little predictive or synthesizing power and will not be more fully developed here.

In summary, we find good agreement between the expected and observed properties of the primary hot spot itself. However, most of these properties would also be true in other models, and thus they do not help decide among competing

pictures. The only definitive test would be detection of the jet leading into the hot spot, but this has not yet been seen. A further difficulty with the above picture is that we must accept the overall symmetry of the hot spot region, its orientation with respect to the southern lobe (see below), and the existence, central placement, and magnetic field structure of the H as accidental features.

d) Axisymmetric Flow Picture

In this picture, illustrated in Figure 6*b*, we are assuming that the entire observed structure of 3C 33 North is only a few times larger than the incoming jet, and that the flow diverges from the on-axis terminal shock. The currently most detailed and useful simulations for comparison with observations are those of SNWS and CNB. In the latter work, CNB examine the total intensity and polarization structure of jets/hot spots with initially helical fields, over a range of helix pitch angles and line-of-sight viewing angles. We will start by looking at the geometrical and magnetic field structures of 3C 33 North, before discussing the less certain predictions of synchrotron emissivity. Again, we note the assumption that radiating particles are found only within the contact discontinuity.

1. *Shape of the leading edge.*—SNWS showed the dramatic time evolution experienced by the contact discontinuity. Most of the time, the leading edge has a flat appearance or is centrally dimpled. The CNB calculations are shown at such a time, so that the curved leading edges in their simulations are due to the projection of the circular jet. The elliptical appearance can then be used to estimate the angle of the jet from the line of sight. For 3C 33 North, we estimate this angle at $\approx 50°$, and we will thus compare our observations to parts *c* (60°) of Figures 1–12 of CNB. An alternative geometry, in which the curved leading edge is intrinsic, is also possible but will not be explored here.

2. *Orientation.*—In the absence of deflections to the jet, the structure of the hot spot region will reflect the jet axis. There are two directions of interest in 3C 33. The first is 19°, which defines the source major axis. The second is $11° \pm 2°$, which is the symmetry axis of the parabola-shaped *southern* hot spot (R88). In 3C 33 North, we determined the orientation from the line connecting the two peaks at the extreme opposite edges of the source. We obtain a value of $12° \pm 2°$, identical to the orientation ($+180°$) of the southern hot spot. Overall, 3C 33 thus displays a kind of S-shaped (rotational) symmetry, with the hot spots directed at $\approx 7°$ from the major source axis (see Fig. 7). Standard explanations for rotational symmetry refer to the locus of emission, and therefore they may not be useful in explaining the apparent velocity direction symmetry in 3C 33. In the splash models described above, this symmetry between north and south must be viewed as accidental.

3. *Terminal shock structure.*—In light supersonic flows, the material is strongly decelerated at a terminal shock, raising the density, temperature, and pressure of the fluid. The head of the jet typically expands to 3–4 times the width of the incoming jet (see, e.g., Norman, Winkler, and Smarr 1983). Within the jet, there is often a shocked core, itself about 2 times narrower than the jet. The observed H feature in 3C 33 North (Fig. 1, feature C; and Fig. 4) has a width of $\frac{1}{7}$ of the total size of the hot spot region and is located near the symmetry line, just as expected if it is illuminating the shocked jet core. In addition, the emissivity is seen to rise dramatically downstream (to the north) of this feature, as seen in Figure 5*c*.

Examination of the time history of a Mach 6 jet (Woodward 1988) shows that about $\frac{3}{4}$ of the time this shock is parallel (i.e., normal to the flow, often called a Mach disk). An H-type structure (Mach stem) appears in some of the flow variables, such as vorticity or velocity divergence, where triple shocks form at the ends of the parallel shock. The parallel shock structure evolves into oblique or diamond-shaped shocks and later reforms as the jet propagates. Thus, about $\frac{1}{4}$ of the time, we do not expect to see any parallel terminal shock.

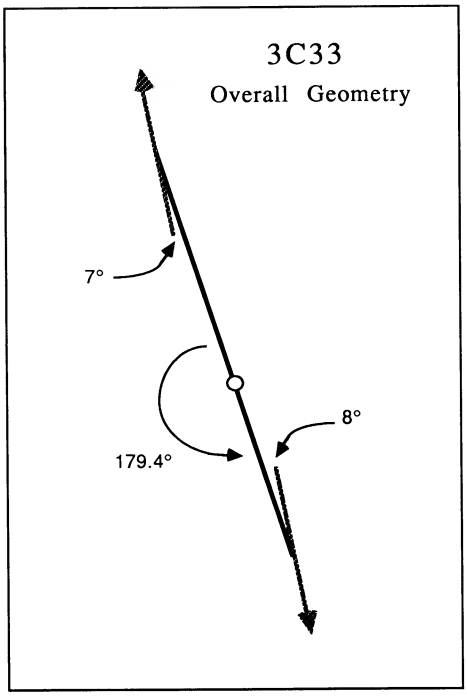

FIG. 7.—Schematic of overall geometry of 3C 33. The vectors at the ends represent the local symmetry directions of the hot spots. The location of the nucleus is indicated by a circle.

4. *Magnetic field transition into hot spot.*—The compression of the flow downstream of the terminal shock leads to an increasing dominance of toroidal field components over axial (poloidal) ones. In CNB, this can be seen as a transition from a magnetic field which first appears longitudinal to the incoming flow, and then becomes transverse (their Figs. 6 and 7, where both poloidal and toroidal components are initially present). Such a transition is seen at the H feature in 3C 33 North (Fig. 4*b* here), although under somewhat different circumstances. The simulation times that CNB selected for display *did not include a parallel shock* (D. Clarke, private communication). However, the compression that takes place at such shocks would also produce a clear axial to toroidal transition. The observed transition strongly supports a change of flow properties at the H feature, independent of the detailed cause.

5. *Magnetic field structure along leading edge.*—Circumferential fields along boundaries are a common feature of observed radio sources as well as in simulations. The presence of either toroidal or poloidal components not in the plane of the sky causes the projected magnetic field directions to appear circumferential (CNB). Figures 6 and 7 again show the closest correspondence to the observed polarization pattern in 3C 33 North. Panels (*a*) and (*b*) of these figures (90° and 75° to the line of sight, respectively) clearly do not produce enough of a circumferential effect to match the observations, and panel (*d*) (30°) produces a circumferential field which

extends throughout the entire hot spot, which is not what we observe. Panel (*c*) (60°), which is the same projection we identified from the shape of the leading edge, once again produces the best correspondence with observations.

Similar circumferential magnetic field results are seen in the simulations of Matthews (1989), although he started with a *random* magnetic field, instead of the ordered one of CNB. This emphasizes the importance of the fluid motions in dominating the ultimate field structures of hot spots through asymmetric compression and shear.

An alternative picture is that 3C 33 North is in the plane of the sky and that the curvature of the leading edge is intrinsic. Whether this edge is the contact discontinuity or bow shock, shear in the flow would create the observed circumferential fields.

6. *Fractional polarization.*—The smaller path lengths at the edge of a source result in less interference along the line of sight and contribute to higher fractional polarizations, although the intrinsic degree of magnetic field order may be uniform throughout the source. Again, asymmetric compression and shearing could increase the field ordering without producing significant limb brightening. The fractional polarization as a function of distance from the center of curvature to the leading edge is shown in Figure 8. For comparison purposes, we have illustrated the interference which can arise from randomly oriented field regions along the line of sight by plotting a curve proportional to (hemispherical path length)$^{-1/2}$.

In summary, the simulations of the terminal regions of axisymmetric jets show a great similarity to 3C 33 North in their structural and polarization properties. However, there is not a good match between the CNB simulations and the emissivity of various features, which we discuss further below.

e) Emissivity

As simulations have become more sophisticated, our expectations regarding the relative synchrotron brightness of various features have changed. That process has not yet converged. The latest simulations of CNB highlighted the importance of the evolution of the magnetic field strength as it was compressed and sheared, as well as the dependence on viewing angle. Matthews (1989) calculated the emissivity with an initially random magnetic field and showed the dramatic changes that can occur when synchrotron losses occur on dynamical time scales. The time and space evolution of the shock structures guarantees, along with the above effects, *that the details of the emissivity are not directly predictable by the overall flow parameters.*

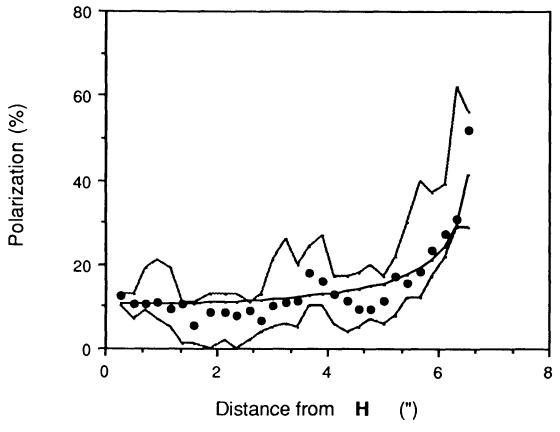

FIG. 8.—Plot of the fractional polarization as a function of (radial) distance from the H feature (feature C) toward the border of the source. Large dots represent the median fractional polarization observed at each distance, while dashed lines indicate the corresponding range in fractional polarizations observed at that distance. The solid line is a simple random-cell model, as described in the text.

For example, *there was no Mach disk present* at the time for which CNB calculated the synchrotron emissivity. Therefore, no H feature could have appeared in their simulated brightness plots. In addition, their convolution results in a resolution which is probably equivalent to a factor of 10 times worse than the observations presented here, removing any small-scale features.

Two-dimensional simulations such as CNB also do not allow any shearing of the toroidal field component, which does appear in the three-dimensional simulations of Arnold and Arnett (1986). This will probably have a significant effect on the emissivity calculations because of the resulting shearing of the magnetic fields. The ordered fields in the CNB calculations also result in a local brightness minimum at the location where we see two bright spots (A and B). Random fields, such as used by Matthews, show that these regions can appear bright due to the long path lengths at these locations.

Although we have assumed no local acceleration of relativistic particles in the discussion so far, such acceleration may be important at the Mach disk (Webb, Drury, and Biermann 1984). Taking the emissivity of the diffuse region to the South (see Fig. 5) as an upper limit to the emissivity of any incoming jet, we find an emissivity increase of ≈ 100 at the H (see Fig. 4*c* and Table 1). Such increases can be realized through compression alone (Rudnick 1988; Scheuer 1989), and particle acceleration is therefore not necessary to explain the current observations. However, studies of spectral index behavior and especially optical synchrotron emission (Crane, Stockton, and Saslaw 1987; Meisenheimer and Röser 1986) in hot spots (including 3C 33 South) show that particle acceleration does occur.

The origin of the emissivity profile through the H feature (Fig. 4*c*) is not clear at present. The on-axis pressure actually drops before the terminal shock in the numerical simulations, whereas we see a gradual rise in emissivity coming into the H feature. In addition, the fluid pressure should plateau downstream of the shock, then perhaps fall slowly as the flow diverges. Instead, we see a sharp drop in brightness downstream of the H feature before it reaches a plateau. Both of these features—the precursor and a local maximum in brightness—can develop if particle acceleration is important and the shock can be mediated by the relativistic particle pressure (T. W. Jones, private communication). Higher dynamic range observations, to remove the upstream background emissivity, and spectral index observations are in progress and will help to examine these questions.

The H feature local maximum might also be intrinsically much narrower than we observe, because of projection effects. Although the H feature cannot be cleanly isolated from the surrounding emission, the width of the peak in Figure 4*c* is at least 0".9. If this width arose from an infinitely thin, circular Mach disk, the projection angle would be $\approx 50°$ from the line of sight, the same angle derived above from the shape of the leading edge.

For completeness, we mention again that neither relativistic beaming effects or emission from outside the contact discontinuity were included in our discussions or those of CNB.

In summary, we find a good correspondence between the structural and polarization properties of 3C 33 North and those expected from the head of an axisymmetric jet. The mismatch in emissivities between our observations and the simulations of CNB suggests that shear of the toroidal field and particle acceleration may be important.

f) *Other Hot Spots*

The current set of observations was undertaken to see if another bow shock model, like that proposed for the strongly limb brightened, parabolic shaped 3C 33 South, could be used to describe 3C 33 North, which has about $\frac{1}{2}$ the luminosity within the first 10 kpc. Instead, the structures in these two hot spots turned out to be very different (see Rudnick 1989), despite the fact that they are very well aligned with the nucleus, only 30% different in their distance to the nucleus, and have post–hot spot lobe luminosities that are within 19% of each other. These large-scale similarities make it very difficult to explain the differences between the two hot spots in terms of either

a) differences in the overall flow properties of the two jets, or

b) large-scale environmental influences.

Small-scale irregularities (≤ 10 kpc) could produce differences, but they would also destroy the alignment and the simple, symmetric structures in the two lobes. Relativistic beaming does not seem likely to explain the difference in morphologies, although no one has made a serious attempt at this kind of model. After examining movies of jet simulations (Woodward 1988), it is also very difficult to picture an evolutionary sequence that would connect these two very different structures.

This problem is not unique to 3C 33. As highlighted in Rudnick and Edgar (1984), the hot spots on opposite sides of strong radio sources are rarely identifiable as belonging to the same parent galaxy. Yet over the long term, the diffuse lobes shows us that the energy supply and environmental factors are very similar on the two sides. At present, we feel there are no good answers to this dilemma, and our results on the hot spots in 3C 33 are an especially good example of the problem.

IV. SUMMARY

We have presented high-resolution observations of the structure and polarization of 3C 33 North, which show it to have a mushroom cap appearance with bright oppositely placed features and a centrally located H-shaped structure. No incoming jet has yet been detected.

The structure of 3C 33 North was interpreted in the context of two models. The first model was that of a primary hot spot plus secondary or "splash" region. The properties of the peak in 3C 33 North agree well with those of other primary hot spots, although some problems arise in the interpretation of the secondary structures.

The second model, developed in more detail, described the whole of 3C 33 North as the terminal region of an axisymmetric jet. The structural and polarization properties agree well with the results of numerical simulations, although the emissivities of various features are not well explained.

The emissivities of hot spots will vary significantly on dynamical time scales of the incoming flow and are subject to a number of effects which have not yet been included in simulations, such as toroidal shear and particle acceleration.

Comparing 3C 33 North and South, we find completely different structures, whereas the overall properties and alignment of the two sides are quite similar. There is currently no good explanation for creating such distinct but simple and symmetric structures from the same parent galaxy.

Our comprehensive evaluation of two distinct, detailed models of flow patterns in the hot spot 3C 33 North showed that both could be used to explain many of the observed features. Readers must remain critical of analyses which promote only one flow picture, especially when less detailed observations are available.

We are pleased to acknowledge discussions and/or comments on the text from David Clarke, Tom Jones, Mike Norman, and Paul Woodward. Jeff Pedelty assisted in the original observations. We also thank Robert Laing for his animated criticism of the axisymmetric interpretation, which resulted in a more detailed examination of the observational evidence. This work was partially funded by NSF grant AST 87-15949 at the University of Minnesota.

REFERENCES

Arnold, C. N., and Arnett, W. D. 1986, *Ap. J. (Letters)*, **305**, L57.
Baars, W. J. M., Genzel, R. Pauliny-Toth, I. I. K., and Witzel, A. 1977, *Astr. Ap.*, **61**, 99.
Bridle, A. H. 1986, *Canadian J. Phys.*, **64**, 353.
Carilli, C., Dreher, J. W., and Perley, R. A. 1989, in *Hot Spots in Extragalactic Radio Sources*, ed. K. Meisenheimer and H.-J. Röser (Berlin: Springer-Verlag), p. 51.
Clarke, D. A., Norman, M. L., and Burns, J. O. 1989, *Ap. J.*, **346**, 700 (CNB).
Crane, P., Stockton, A., and Saslaw, W. C. 1987, *Astr. Ap.*, **183**, 16.
Dreher, J. W., Carilli, C. C., and Perley, R. A. 1987, *Ap. J.*, **316**, 611.
Fanaroff, B. L., and Riley, J. M. 1974, *M.N.R.A.S.*, **167**, 31p.
Hargrave, P. J., and McEllin, M. 1975, *M.N.R.A.S.*, **173**, 37.
Hargrave, P. J., and Ryle, M. 1974, *M.N.R.A.S.*, **166**, 305.
Icke, V. 1989, *Astr. Ap.*, submitted.
Laing, R. L. 1989, in *Hot Spots in Extragalactic Radio Sources*, ed. K. Meisenheimer and H.-J. Röser (Berlin: Springer-Verlag), p. 27.
Lonsdale, C. J. 1989, in *Hot Spots in Extragalactic Radio Sources*, ed. K. Meisenheimer and H.-J. Röser (Berlin: Springer-Verlag), p. 219.
Lonsdale, C. J., and Barthel, P. D. 1986, *Ap. J.*, **92**, 12.
Matthews, A. P. 1989, in *Hot Spots in Extragalactic Radio Sources*, ed. K. Meisenheimer and H.-J. Röser (Berlin: Springer-Verlag), p. 219.
Matthews, T. A., Morgan, W. W., and Schmidt, M. 1964, *Ap. J.*, **140**, 35.
Meisenheimer, K., and Röser, H.-J. 1986, *Nature*, **319**, 459.
Norman, M. L., Winkler, K.-H., and Smarr, L. 1983, in *Astrophysical Jets*, ed. A. Ferrari and A. G. Pacholcyzk (Dordrecht: Reidel), p. 228.
Rudnick, L. 1988, *Ap. J.*, **325**, 189 (R88).
———. 1989, in *Hot Spots in Extragalactic Radio Sources*, ed. K. Meisenheimer and H.-J. Röser (Berlin: Springer-Verlag), p. 61.
Rudnick, L., and Edgar, B. K. 1984, *Ap. J.*, **279**, 74.
Scheuer, P. A. 1989, in *Hot Spots in Extragalactic Radio Sources*, ed. K. Meisenheimer and H.-J. Röser (Berlin: Springer-Verlag), p. 159.
———. 1982, in *IAU Symposium 97, Extragalactic Radio Sources*, ed. D. S. Heeschen and C. M. Wade (Dordrecht: Reidel), p. 163.
Simkin, S. 1979, *Ap. J.*, **234**, 56.
Smith, M. D., Norman, M. L., Winkler, K.-H. A., and Smarr, L., 1985, *M.N.R.A.S.*, **214**, 67 (SNWS).
Webb, G. M., Drury, L. O'C., and Biermann, P. 1984, *Astr. Ap.*, **137**, 185.
Williams, A. G., and Gull, S. F. 1985, *Nature*, **313**, 34.
Woodward, P. R. 1988, in *Supercomputer Simulations in Astrophysics* (University of Minnesota: Department of Independent Study videotapes).

MARTHA ANDERSON and LAWRENCE RUDNICK: Department of Astronomy, University of Minnesota, 116 Church Street SE, Minneapolis, MN 55455